Video Article

Indacenodithienothiophene-Based Ternary Organic Solar Cells: Concept, Devices and Optoelectronic Analysis

Nicola Gasparini[1], Amaranda García-Rodríguez[2], Athanasios Katsouras[3], Apostolos Avgeropoulos[3], Georgia Pagona[4,5], Vasilis G. Gregoriou[4,5], Christos L. Chochos[3,4], Sybille Allard[2], Ulrich Scherf[2], Christoph J. Brabec[1,6], Tayebeh Ameri[1]

[1]Institute of Materials for Electronics and Energy Technology (I-MEET), Friedrich-Alexander-University Erlangen-Nuremberg

[2]Macromolecular Chemistry Group (buwmakro) and Institute for Polymer Technology, Bergische Universität Wuppertal

[3]Department of Materials Science Engineering, University of Ioannina

[4]Advent Technologies SA

[5]National Hellenic Research Foundation (NHRF)

[6]Bavarian Center for Applied Energy Research (ZAE Bayern)

Correspondence to: Nicola Gasparini at nicola.gasparini@fau.de

URL: http://www.jove.com/video/54007
DOI: doi:10.3791/54007

Keywords: ternary organic solar cells, indacenodithienothiophene, photo-CELIV, Transient Photovoltage, Charge extraction, Photo-induced absorption spectroscopy

Date Published: 10/30/2016

Citation: Gasparini, N., García-Rodríguez, A., Katsouras, A., Avgeropoulos, A., Pagona, G., Gregoriou, V.G., Chochos, C.L., Allard, S., Scherf, U., Brabec, C.J., Ameri, T. Indacenodithienothiophene-Based Ternary Organic Solar Cells: Concept, Devices and Optoelectronic Analysis. *J. Vis. Exp.* (), e54007, doi:10.3791/54007 (2016).

Abstract

We report on a novel ternary bulk-heterojunction solar cell by implementing a novel conjugated polymer (ADV-2) containing alternating pyridyl[2,1,3]thiadiazole (PT) between two different donor fragments, dithienosilole (DTS) and indacenodithienothiophene (IDTT), into a host system of indacenodithieno[3,2-*b*]thiophene,2,3-bis(3-(octyloxy)phenyl)quinoxaline (PIDTTQ) and [6,6]-phenyl C71 butyric acid methyl ester ($PC_{71}BM$). A clear absorption contribution in the near infrared (NIR) region leads to a power conversion efficiency (PCE) exceeding 4.6% in ternary device processed by doctor blading in air, fully avoiding any thermal treatment. Current-voltage (J-V) characteristics, external quantum efficiency (EQE) spectrum, charge extraction (CE) as well as photo-induced absorption (PIA) spectroscopy reveal the higher charge carrier generation in the ternary devices compared to the reference binary cells. Despite an enhancement of about 20% in the short circuit current density (J_{sc}), the lower fill factor (*FF*) achieved in PIDTTQ:ADV-2:$PC_{71}BM$ ternary system limits the solar cell performance. With the complementary use of photoinduced charge carrier extraction by linearly increasing voltage (photo-CELIV) and transient photovoltage (TPV) measurements, we found that the ternary cells suffer from a lower mobility-lifetime (μτ) product, adversely impacting the *FF*. However, the significant improvement of light harvesting in the NIR region, compensating the transport losses, results in an overall power conversion efficiency enhancement of ~7% for ternary blends as compared to the PIDTTQ: $PC_{71}BM$ devices.

Introduction

During the last decades, the power conversion efficiency (PCE) of organic bulk-hetorojunction (BHJ) solar cells based on donor/acceptor blends surpassed the 10% threshold, mainly due to the discovery of novel materials as well as device structure engineering.[1-6] Nowadays, one of the main challenges in order to further boost the PCE of organic solar cells is to achieve better absorption match to the solar irradiance spectrum, by extending the narrow absorption window of organic polymers. In this regards, two main concepts have been developed: tandem and ternary organic solar cells.[7-17] The former are based on a complex multi-layer stack with the main challenge of designing a robust solution-processed intermediate layer.[18] The latter, made of two donors and one acceptor, mixed together in a unique solution, overcomes the complexities of the tandem device architecture, maintaining the easy processability of a single junction organic BHJ solar cell.[19-25] To date, polymers,[20] small molecules,[21] dyes,[26] quantum dots[27] and fullerene derivates,[23] have been adopted as "guest" in the polymer-fullerene "host" system.

In addition to the need for donor materials with the complementary absorption, one of the key points to surpass the performance of binary cells in ternary devices is to find donor materials with compatible physical and chemical natures.[20] This can prevent the formation of recombination centers, or morphological traps, that deteriorate the photovoltaic properties.[28,29]

Here, we report a ternary organic solar cell system processed in air that shows a pronounced sensitization effect, resulting in a power conversion efficiency of more than 4.6%. As a sensitizer, we incorporate the near infrared (NIR) polymer ADV-2 that contains alternating pyridyl[2,1,3]thiadiazole (PT) between two different donor fragments, dithienosilole (DTS) and indacenodithienothiophene (IDTT), into a host system of indacenodithieno[3,2-b]thiophene,2,3-bis(3-(octyloxy)phenyl)quinoxaline (PIDTTQ)[30] blended with [6,6]-phenyl C71 butyric acid methyl ester ($PC_{71}BM$). In fact, in order to have components with a similar chemical nature in the ternary blend system, we used two polymers with the same backbone unit of indacenodithienothiophene for the host and the guest donors. We studied the aforementioned ternary system by employing various optoelectronic techniques such as current-voltage (J-V) characteristics, external quantum efficiency (EQE), photoinduced charge carrier extraction by linearly increasing voltage (photo-CELIV), charge extraction (CE), transient photovoltage (TPV) measurements and photo-induced absorption (PIA) spectroscopy.

Protocol

1. Planning of experiment

1. Identify two donor copolymers with complementary absorption in the visible-NIR range and with suitable energy levels in comparison with the fullerene derivative acceptor ($PC_{71}BM$).

2. Synthesis of M1

1. Add a 10 mL freshly distilled toluene solution containing 5,5'-bis(trimethylstannyl)-3,3'-di-2-ethylhexylsilylene-2,2'-bithiophene (0.372 g, 0.5 mmol, the quantity as well as the representative mmol corresponds to 5,5'-bis(trimethylstannyl)-3,3'-di-2-ethylhexylsilylene-2,2'-bithiophene), 4,7-dibromo-[1,2,5]thiadiazolo[3,4-*c*]pyridine (0.295 g, 1 mmol) and $Pd(PPh_3)_4$ (57.8 mg, 0.05 mmol) into a microwave tube under the protection of nitrogen.
2. Perform the Stille coupling with the following procedure: 120 ^{o}C for 10 min, 140 ^{o}C for 10 min, 160 ^{o}C for 10 min and 170 ^{o}C for 40 min (microwave step-wise).
3. Cool down the reaction to room temperature, and extract with chloroform (100 mL × 3) in a separatory funnel. Wash with deionized water (100 mL × 3) and dry with anhydrous magnesium sulfate.
4. Using a rotary evaporator, remove the solvent under reduced pressure. Separate the mixture by adding the solute directly to a silica column (25 mm inner diameter x 300 mm length) with hexane/chloroform (from 100/0 to 0/100 in v/v) to give 0.49 g of dark-purple solid (92% yield).

3. Synthesis of ADV-2:

1. Dissolve dibromo monomer M1 (180 mg, 1 equiv) and distannyl monomer M2 (286 mg, 1 equiv) in 1 mL toluene in a microwave vial. Fix the volume of the solvent and the quantity of the monomers to 0.025 M in concentration for each polymerization procedure.
2. Add $Pd_2dba_3{\cdot}CHCl_3$ (4.4 mg, 0.02 equiv) and tri(*o*-tolyl)phosphine ($P(o\text{-tol})_3$) (2.6 mg, 0.04 equiv) in the reaction mixture and stir at 120 °C under argon atmosphere for 48 h.
3. Purify the polymer by precipitation in methanol in a beaker, and then filter through a thimble and Soxhlet extract with methanol, acetone, ethyl acetate, chloroform and dichlorobenzene (DCB) in sequential order. Use 20% in excess of the volume of the polymeric solution.
4. Collect the DCB fraction with a rotary evaporator and remove the solvents under reduced pressure.
5. Isolate the polymer by precipitation into methanol in a beaker. Use 20% excess in volume. Filter and finally dry under high vacuum to give ADV-2 as a blue solid in 79% yield (142.2 mg).

4. Preparation of material solution

1. Prepare 10 mg/mL solution of indacenodithieno[3,2-b]thiophene,2,3-bis(3-(octyloxy)phenyl)quinoxaline in 1,2 dichlorobenzene (DCB).
2. Prepare 10 mg/mL solution of ADV-2 in DCB.
3. Prepare 40 mg/mL solution of [6,6]-phenyl C70 butyric acid methyl ester ($PC_{71}BM$) in DCB.
4. Stir all the solutions overnight on hot plate at 80 °C.

5. Preparation of bulk-heterojunction(BHJ) solar cells

1. Mix the solutions with different composition ratios (Table 1), keeping the total solution concentration at 20 mg/mL; add 3% v/v 1-Chloronaphtalene (CN). Stir the ternary as well as binary solutions 1 hour at 80 °C.
2. Clean the pre-structured indium tin oxide (ITO) substrates in acetone and isopropyl alcohol in an ultrasonic bath for 10 minutes each.
3. After drying, coat the substrates with 40 nm of zinc oxide (ZnO) with a doctor-blade.[30]
    1. Coat the aforementioned (Table 1) active layer materials with a doctor-blade. Set the temperature of doctor blade at 80 °C, the gap between the blade and the substrate at 400 µm, use 60 µL of solution and adjust the coating speed (10 mm/s) in order to have approximately 100 nm active layer thickness.
4. To complete the fabrication of the devices, transfer the substrate in glove-box filled with nitrogen.
5. In an ultra-vacuum chamber, thermally evaporate 10 nm of MoOx and 100 nm of Ag through a mask with a 10.4 mm^2 active area opening and under a vacuum of 2×10^{-6} mbar.

6. Electrical and optical characterization of solar cells

1. **J-V characteristics:**
    1. Measure the J-V characteristics of the BHJ devices between -2 V to 2 V under darkness using a source measurements unit according to manufacturer's protocol. Scan the voltages between -2 V and 2 V with steps of 20 mV to record the corresponding current (I). Calculate the current density (J) by the equation J=I/A, where A is the area of the solar cells (here, 10.4 mm^2).
    2. Provide illumination with a solar simulator with AM1.5G spectrum at 100 mW cm^{-2}. Measure the J-V characteristics of the BHJ devices between -2 V to 2 V under light conditions in ambient air using a source measurements unit according to manufacturer's protocol.
        1. Scan the voltages between -2 V and 2 V with steps of 20 mV to record the corresponding current (I). Calculate the current density (J) by the equation J=I/A, where A is the area of the solar cells (here, 10.4 mm^2).

2. **Absorption spectra and External Quantum Efficiency (EQE) measurements:**
    1. Measure the absorption spectra of the solar cells on film with a UV-VIS spectrometer according to manufacturer's protocol.
    2. Calibrate the EQE setup with a silicon diode reference cells between 350 and 900 nm.
    3. Measure solar cells EQEs using an integrated system between 350 and 900 nm. [30]

3. **Photoinduced charge carrier extraction by linearly increasing voltage (photo-CELIV):**[30]
    1. Illuminate the devices with a 405 nm laser diode.
    2. Connect the solar cells with the oscilloscope with BNC cable. Record the current transient across an internal 50Ω resistor of an oscilloscope[30].
    3. After a variable delay time (delay time reflects the time passing from the laser pulse to the start of the voltage ramp, can vary between 1us to 1-10 ms), apply a linear extraction ramp via a function generator. Set the ramp, which is 60 µs long and 2 V in amplitude, to start with an offset matching the V_{oc} of the cell for each delay time.

4. **Transient Photo-Voltage (TPV):**[31]
    1. Use two lasers at 405 nm, one as background illumination and the other one for creating voltage perturbation.
    2. Connect the solar cell to an oscilloscope with BNC cable and adjust the intensity of the background illumination to reach the open circuit condition.
    3. Adjust the laser intensity pulse to keep the voltage perturbation below 10 mV, typically at 5 mV. After the pulse, the voltage decays back to its steady state value in a single exponential decay.
    4. Change intensity of background illumination in a range of 0.1 to 4 suns.
    5. Record the transient with the oscilloscope.

5. **Charge extraction (CE):**[31]
    1. Use a 405 nm laser diode for background illumination.
    2. Connect the solar cell to an oscilloscope with BNC cable and adjust the intensity of the background illumination to reach the open circuit condition.
    3. Turn off the laser and trigger the bilateral switch in order to switch the solar cell from open-circuit to short-circuit (50 Ω) conditions within less than 50 ns.
    4. Record the transient with the oscilloscope.

6. **Photo-induced spectroscopy (PIA):**
    1. Place the solar cell in a cryostat in order to reach a temperature of 10 K and a pressure of 5×10^{-7} mbar.
    2. Check the optical alignments for a 532 nm Nd:YAG laser (as pump) and a UV-VIS lamp light (as probe), focused on the same position on the sample.
    3. Turn off the laser and measure the sample transmittance by a standard lock-in technique under the UV-VIS lamp light which is modulated by a mechanical chopper.
    NOTE: In this method the excitation (laser PUMP) is done by using a green laser (λ=532 nm), which is modulated by a mechanical chopper. The sample is additionally illuminated by a monochromated light beam ("probe") of a white light source. First the sample's transmittance and the sample's photoluminescence is measured. The measured signal is analyzed with a lock-in amplifier using the chopper frequency as the reference signal, allowing a very precise quantification of the change in absorption induced by the pump-light. Using various detectors (Si, Ge) a broad wavelength region ranging from 400 nm up to 1800 nm can be analyzed. Varying the material composition, material dependent effects can be characterized.
    4. Turn off the lamp and turn on the laser beam, modulated by a mechanical chopper.
    5. Measure the photoluminescence of the solar cells through the standard lock-in technique.
    6. Turn on the lamp and then measure the PIA spectrum by a standard lock-in technique under modulated laser pulse.

Representative Results

Figure 1 shows 1H and 13C NMR spectra of M1 (a-b, respectively) and ADV-2 (c-d, respectively) with their respectively list of peaks. **Figure 2** shows the synthetic route for the low band gap donor-acceptor copolymer ADV-2. **Figure 3** shows the absorption spectrum of ADV-2 in DCB solution and as solid. The copolymer for both cases shows a single band in the high energy region which is assigned to a localized π −π* transition and another absorption band in the low energy region (up to 1000 nm) which is assigned to an intramolecular charge transfer transition. The maximum of the near infrared absorption band of ADV-2 in the solid state is bathochromic shifted (738 nm) in comparison to the corresponding UV-Vis solution (695 nm). The optical band gap energy estimated from the absorption edge of film spectrum was estimated to be 1.87. Based on the onsets of the oxidation and reduction peaks in cyclic voltammetry measurements, the electrochemical HOMO and LUMO energies were estimated to be −5.34 and −3.71 eV, respectively, corresponding to an electrochemical band gap energy of 1.63 eV.

Figure 4a shows the device architecture used in this work, based on ITO/ZnO/active layer/MoO_x/Ag. PIDTTQ has been previously presented in the literature.[30] All the solution processed layers are doctor-bladed in air. **Figure 4b** and **4c** depict the energy levels of the polymers and the fullerene derivate, measured by cyclic-voltammetry (CV) and the chemical structure of the materials used, respectively.

Figure 5a shows the current-voltage characteristics of the binary PIDTTQ:PC_{71}BM (1:2 wt/wt) as well as ternary PIDTTQ:ADV-2:PC_{71}BM (different composition) under 1 sun illumination (100 mW cm^{-2}). In agreement with previous reports binary cells delivered a PCE of 4.35% with an open circuit voltage (V_{oc}) of 0.84V, a short circuit current (J_{sc}) of 8.62 mA cm^{-2} and a fill factor (*FF*) of 60%. Adding 15 wt% of the NIR sensitizer, the ternary device delivered the highest performance with a J_{sc} of 10.60 mA cm^{-2}, V_{oc} of 0.84 V and *FF* of 52%, resulting the overall power conversion efficiencies of 4.6%. As shown in **Table 1**, the J_{sc} increased monotonically by increasing the of ADV-2 content up to 15 wt%, due to the better photon harvesting of the ternary system in the NIR region. For PIDTTQ:ADV-2:PC_{71}BM (0.85:0.15:2) ternary blend a J_{sc} improvement of ~20% was achieved as compared to PIDTTQ:PC_{71}BM binary system. Notably, the V_{oc} obtained in the ternary cells are identical to the binary PIDTTQ:PC_{71}BM, reflecting a cascade alignment between the HOMO and LUMO energy levels of the three components (**Figure 4b**).[25] However,

we observed a continuously decrease in *FF* by introducing higher amount of ADV-2, which can be attributed to the undesired morphology of the ternary blends. We further measured external quantum efficiency (EQE) spectra of OPV devices made from PIDTTQ:ADV-2:$PC_{71}BM$, PIDTTQ:$PC_{71}BM$ and ADV-2:$PC_{71}BM$ (**Figure 5b**). Increasing the ADV-2 content, the EQE showed improved photoresponse at 700-800 nm region, which is the origin of the enhanced J_{sc}. We note that the integrated EQE for these devices matches the measured short circuit current within a margin of 5%.

In order to understand the lower *FF* obtained in the ternary BHJ solar cells we first studied the charge transport properties by employing the technique of photoinduced charge carrier extraction by linearly increasing voltage (photo-CELIV).[32-34] From the measured photocurrent transients, the charge carrier mobility (μ) was calculated using the following equation:

$$\mu = \frac{2d^2}{3At_{max}^2\left[1+0.36\frac{\Delta j}{j(0)}\right]} \; if \; \Delta j \leq j0, \quad (1)$$

where d is the active layer thickness, A is the voltage rise speed A=dU/dt, U is the applied voltage, t_{max} is the time corresponding to the maximum of the extraction peak, and j(0) is the displacement current.[32] **Figure 6a** shows the transient recorded by applying a 2V/60 μs linearly increasing reverse bias and a delay time (t_d) of 10 μs. From analysis of the photo-CELIV traces the charge carrier mobility values of 1.13×10^{-4} $cm^2V^{-1}s^{-1}$, 8.54×10^{-5} $cm^2V^{-1}s^{-1}$, 7.53×10^{-5} $cm^2V^{-1}s^{-1}$ and 7.42×10^{-5} $cm^2V^{-1}s^{-1}$ were calculated for PIDTTQ:$PC_{71}BM$ (1:2), PIDTTQ:ADV-2:$PC_{71}BM$ (0.90:0.10:2), PIDTTQ:ADV-2:$PC_{71}BM$ (0.85:0.15:2), PIDTTQ:ADV-2:$PC_{71}BM$ (0.80:0.20:2) devices, respectively. The lower charge carrier mobilities measured with Photo-CELIV technique are in agreement with the lower *FFs* obtained for the ternary cells. We then analyzed the lifetime of charge carriers by employing transient photovoltage technique (TPV).[35,36] The samples were connected to the terminal of an oscilloscope with the input impedance of 1 MΩ and illuminated with a continuous background laser to keep the samples at V_{oc} condition. A small voltage perturbation was applied using a blue laser (λ=405 nm). The pulse intensity was adjusted to keep the height of the photovoltage transient smaller than 10 mV resulting in a voltage transient with amplitude $\Delta V \ll V_{oc}$. The measured transient decays show the form of single exponentials, as expected for the pseudo-first order kinetic.[35]

$$\frac{d\Delta V}{dt} \propto \frac{d\Delta n}{dt} = -k_{eff} = -\frac{\Delta n}{\tau_{\Delta n}} \quad (2)$$

V is the photovoltage, t is the time, Δn is change in the density of photogenerated carriers due to the perturbation pulse, k'_{eff} is the pseudo-first order rate constant and $\tau_{\Delta n}$ is the carrier lifetime. **Figure 6b** depicts normalized photovoltage decays as a function of time for the binary and ternary devices. As reported in **Table 2**, quite similar charge carriers lifetime of 6.72 μs, 7.35 μs and 7.23 μs were achieved for PIDTTQ:$PC_{71}BM$ (1:2), PIDTTQ:ADV-2:$PC_{71}BM$ (0.90:0.10:2), PIDTTQ:ADV-2:$PC_{71}BM$ (0.85:0.15:2), respectively, suggesting that these ternary blends are not limited by the short lifetime of charge carriers.[37] Otherwise, a reduce τ of 4.72 μs is observed for the PIDTTQ:ADV-2:$PC_{71}BM$ (0.80:0.20:2) based ternary system. Combining the results of Photo-CELIV and TPV measurements we were able to calculate the mobility-lifetime product *(μτ)*. As presented in **Table 2**, μτ decrease from 7.59×10^{-10} for PIDTTQ:$PC_{71}BM$ (1:2) to 6.72×10^{-10}, 5.44×10^{-10} and 3.50×10^{-10} cm^2 V^{-1} for, PIDTTQ:ADV-2:$PC_{71}BM$ (0.90:0.10:2), PIDTTQ:ADV-2:$PC_{71}BM$ (0.85:0.15:2) and PIDTTQ:ADV-2:$PC_{71}BM$ (0.80:0.20:2), respectively, owing to the poorer transport properties of the ternary systems compared to the binary reference device.

To have a better insight into the charge photogeneration in the ternary blends, we employed the charge extraction (CE) and photoinduced absorption (PIA) spectroscopy. In CE measurements the samples were illuminated under a continuous background laser to keep it at V_{oc} condition. A nanosecond switch was used to sweep the photocurrent from open circuit to short circuit condition. The charge carrier density (*n*) was calculated based on the transient decay (**Figure 7a**).[31] In agreement with the J_{sc} values obtained, we calculated *n* as 2.97×10^{16}, 3.02×10^{16}, 3.66×10^{16} and 1.15×10^{16} cm^{-3} for PIDTTQ:$PC_{71}BM$ (1:2), PIDTTQ:ADV-2:$PC_{71}BM$ (0.90:0.10:2), PIDTTQ:ADV-2:$PC_{71}BM$ (0.85:0.15:2) and PIDTTQ:ADV-2:$PC_{71}BM$ (0.80:0.20:2) devices, respectively (**Table 2**). Furthermore, the charge generation mechanism in the BHJ solar cells was studied with PIA spectroscopy.[38,39] We utilized a 532 nm laser for pump and a UV-VIS lamp for probing. **Figure 7b** depicts the PIA spectra of binary and ternary devices measured under 60 mW cm^{-2} pump intensity at 10 K. All spectra showed a pronounced transmission minimum (bleach) around 1.81 eV and a photoinduced absorption feature around 1.24 eV. The ternary blends showed a novel bleaching feature around 1.55 eV. We ascribe the two transmission maxima at 1.81 eV and 1.55 eV to the photobleaching of the electronic ground states of PIDTTQ and ADV-2, respectively. As shown in Figure 6b, a higher polaron signal was observed for the PIDTTQ:ADV-2:$PC_{71}BM$ (0.90:0.10:2), PIDTTQ:ADV-2:$PC_{71}BM$ (0.85:0.15:2) ternary devices compared to the binary cell, confirming the higher charge photogeneration by adding 10-15% of ADV-2 into the PIDTTQ:$PC_{71}BM$ host system.

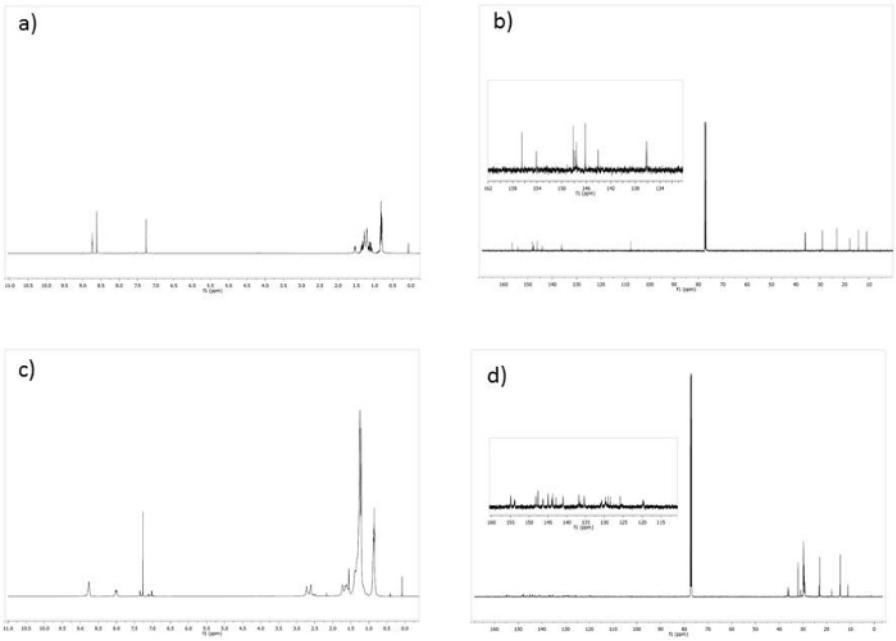

Figure 1 NMR of the NIR polymer. 1H and 13C NMR spectra of M1 (a-b, respectively) and ADV-2 (c-d, respectively).

Synthesis of M1:

^{1}H-NMR (600 MHz, $CDCl_3$), δ (ppm): 8.75 (t, 2H, *J* = 8.76 Hz), 8.63 (s, 2H), 1.55 (q, *J* = 1.53, 2H), 1.38-1.09 (m, 20H), 0.84-0.81 (m, 12H). ^{13}C-NMR (151 MHz, $CDCl_3$), δ (ppm): 156.52 (C), 154.12 (C), 148.12 (C), 147.85 (C), 147.60 (C), 146.16 (CH), 144.10, 136.18 (CH), 107.77, 36.22 (CH), 35.97(CH_2), 29.17 (CH_2), 29.13 (CH_2), 23.15 (CH_2), 17.86 (CH_2), 14.31 (CH_3), 10.98 (CH_3).
MALDI-TOF: *m/z*: 847.2 (M^+, 100)

Synthesis of ADV-2:

^{1}H-NMR (600 MHz, $CDCl_3$), δ (ppm): 8.80-8.76 (m), 8.04-8.00 (m), 7.36 (dd, *J* = 7.4 Hz), 7.02 (dd, *J* = 7 Hz), 2.73 (s), 2.62 (s), 1.74-1.61 (m), 1.39-1.22 (m), 0.89-0.85 (m). ^{13}C-NMR (151 MHz, $CDCl_3$), δ (ppm): 154.73, 153.71, 153.59, 148.07, 147.45, 146.14, 144.84, 143.76, 143.62, 142.71, 140.85, 136.68, 136.22, 135.28, 130.97, 130.57, 129.54, 129.35, 128.75, 128.21, 125.68, 119.52, 36.13, 35.87, 31.92, 30.81, 30.73, 29.68, 29.60, 29.48, 29.35, 29.28, 29.06, 29.04, 23.07, 22.68, 17.80, 14.22, 14.09, 10.87. GPC (TCB): Mn = 36800 g/mol; Mw = 120600 g/mol; PDI 3.3. Please click here to view a larger version of this figure.

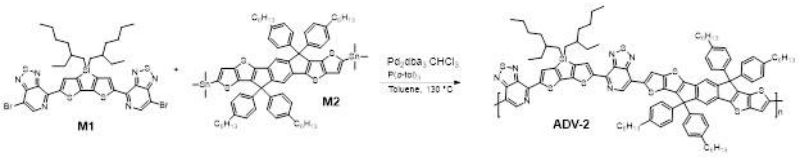

Figure 2: Synthetic route for ADV-2.

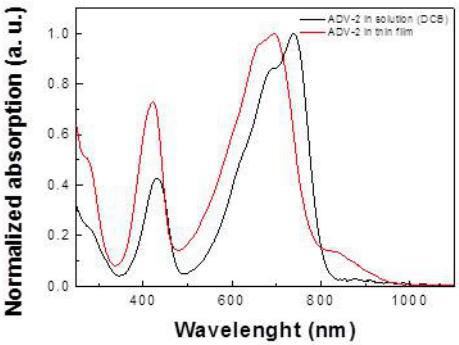

Figure 3: Optical properties of the NIR polymer. Absorption spectra of ADV-2 in solution (DCB) and as thin film.

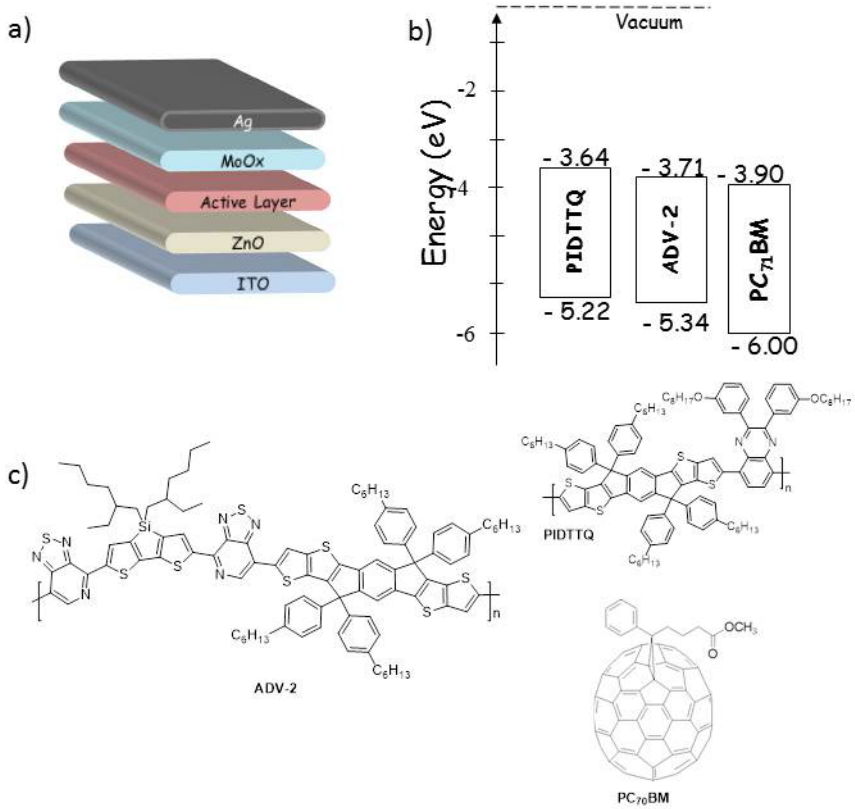

Figure 4: Device representation, electrical and chemical structures of ternary blends. a) Schematic representation of the BHJ solar cells with the layout ITO/ZnO/Active layer/MoOx/Ag. b) Energy levels and c) Chemical structure of the materials used in this work.

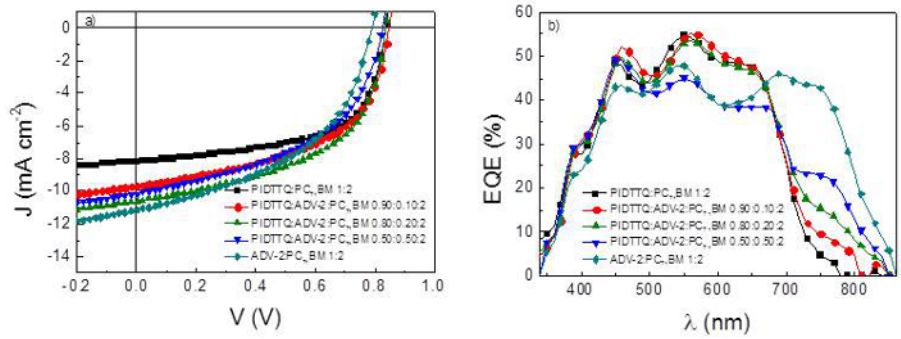

Figure 5: Photovoltaic properties of ternary devices. a) Current density-Voltage characteristics and b) External quantum efficiency curves of PIDTTQ:ADV-2:$PC_{71}BM$ and PIDTTQ:$PC_{71}BM$ solar cells under solar simulator illumination (100 mW cm-2).

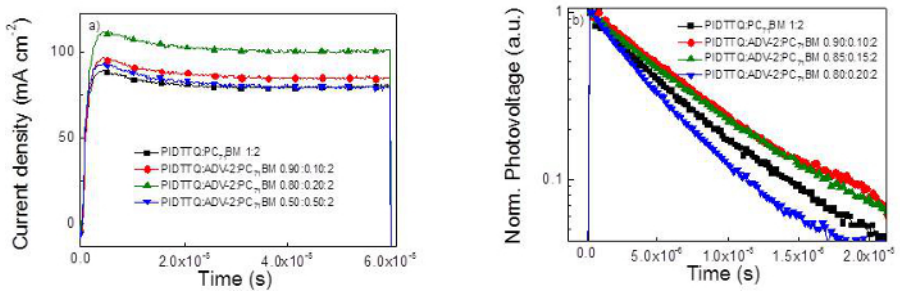

Figure 6: Transport characterizations of ternary blends. a) Time-dependent photo-CELIV traces and b) transient photovoltage (TPV) plots of PIDTTQ:ADV-2:$PC_{71}BM$ and PIDTTQ:$PC_{71}BM$ solar cells.

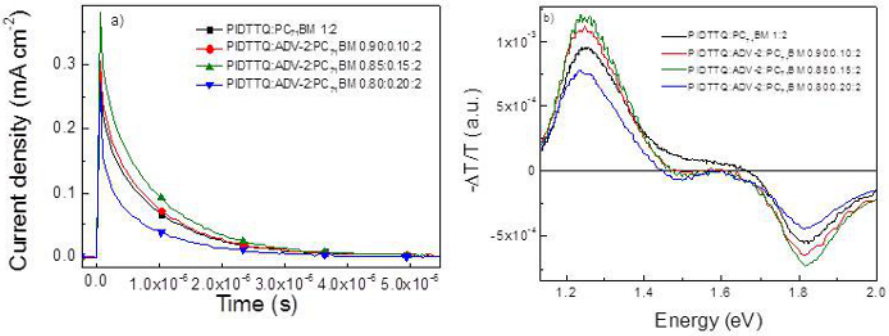

Figure 7: Charge generation ability of ternary devices. a) Charge extraction (CE) traces and b) PIA spectra of PIDTTQ:ADV-2:$PC_{71}BM$ and PIDTTQ:$PC_{71}BM$ solar cells recorded under 60 mW cm^{-2} blue light intensity (l=405 nm) at 10K.

PIDTTQ:ADV-2:$PC_{71}BM$	V_{oc}	J_{sc}	FF	η
	(V)	(mA cm^{-2})	(%)	(%)
1:00:02	0.84 (0.84±0.00)	8.62	60.33 (59.72±0.65)	4.35 (4.24±0.10)
		(8.49±0.23)		
0.90:0.10:2	0.84 (0.84±0.01)	9.69	53.14 (52.48±0.55)	4.29 (4.20±0.10)
		(9.50±0.18)		
0.85:0.15:2	0.84 (0.84±0.01)	10.60 (10.43±0.22)	51.87 (50.64±1.17)	4.63 (4.45±0.19)
0.80:0.20:2	0.84 (0.84±0.01)	10.14 (9.64±0.44)	48.86 (48.64±0.20)	4.04 (3.86±0.17)
0:01:02	0.81	10.87 (10.37±0.41)	46.61 (45.57±0.69)	3.95 (3.79±0.10)
	(0.81±0.00)			

Table 1: Photovoltaic parameters of PIDTTQ:ADV-2:$PC_{71}BM$ and PIDTTQ:$PC_{71}BM$ inverted solar cells under 1 sun illumination (100 mW cm^{-2}). The values are averaged on 12 devices. Composition considered by weight.

PIDTTQ:ADV-2:$PC_{71}BM$	μ	τ	μτ	n
	[$cm^2V^{-1}s^{-1}$]	[s]	[cm^2V^{-1}]	[cm^{-3}]
1:00:02	1.13×10^{-4}	6.72×10^{-6}	7.59×10^{-10}	2.97×10^{16}
0.90:0.10:2	8.54×10^{-5}	7.35×10^{-6}	6.72×10^{-10}	3.02×10^{16}
0.85:0.15:2	7.53×10^{-5}	7.23×10^{-6}	5.44×10^{-10}	3.66×10^{16}
0.80:0.20:2	7.42×10^{-5}	4.72×10^{-6}	3.50×10^{-10}	1.15×10^{16}

Table 2: Summary of calculated charge generation and charge transport parameters of PIDTTQ:ADV-2:$PC_{71}BM$ and PIDTTQ:$PC_{71}BM$ devices: charge carrier (μ), charge carrier density (*n*), charge carrier lifetime (*t*) and mobility-lifetime product (*μ't*).

Discussion

We reported a novel ternary system with a clear contribution in the incident photon-to-current efficiency in the near IR region. A J_{sc} improvement of around 20% was obtained for PIDTTQ:ADV-2:$PC_{71}BM$ (0.85:0.15:2) ternary devices compared to PIDTTQ:$PC_{71}BM$ binary cells. However, the low *FF* limited the performances of the ternary BHJ solar cells.

We found that by adding ADV-2 into the host system of PIDTTQ:$PC_{71}BM$ the *μτ* product is reduced, explaining the lower *FFs*. Despite the poorer transport properties, the complementary results of CE and PIA spectroscopy showed an improved charge generation in PIDTTQ:ADV-2:$PC_{71}BM$ (0.85:0.15:2) ternary solar cells, leading to a PCE of more than 4.6%. We studied the photogeneration ability of the ternary solar cells using these two complementary techniques that require the whole device architecture and just the active layer in CE and PIA measurements, respectively, allowing us to have a better insight into the process, by combining the two methods.

We use common state-of-the-art techniques to fully characterize organic ternary solar cells. In particular we study the transport mechanism of the organic solar cells by employing photo-CELIV and TPV techniques directly on the devices, without the fabrication of any "ad hoc" devices used for instance in space-charge limited current measurements.[40] Moreover, in order to calculate reliable mobility values, we recorded more than 10 curves with different delay time and voltage ramp. Concerning the lifetime calculation, we used TPV as small perturbation method, allowing us to evaluate t at the real operating condition of the solar cells (1 sun condition). With our experimental procedure not only organic solar cells can be characterized but our method can be easily used for inorganic and hybrid solar cells as well.

In conclusion, the combination of the aforementioned techniques allowed us to study the limitation mechanisms of ternary devices compared to the binary solar cells. Overcoming the losses will be a future challenge for the fabrication of high efficiency ternary organic solar cells.

Overall, we reported a combination of standard characterizations, i.e. J-V measurements, with powerful tools such as PIA spectroscopy. The main problem that can arise during the characterization is the device degradation. Therefore, encapsulation as well as characterization in inert condition might preserve the stability of those devices. Having the aforementioned techniques in N_2 or Ar atmosphere, i.e. glove-boxes, will increase the reliability of the device behavior.

Disclosures

The authors have nothing to disclose.

Acknowledgements

This project has received funding from the European Community's Seventh Framework Programme (FP7/2007-2013) under the Grant Agreement n° 607585 project OSNIRO. In addition, this project has received funding from the European Community's Seventh Framework Programme (FP7/2007-2013) under the Grant Agreement no. 331389. C. L. C. acknowledges the financial support of a Marie Curie Intra European Fellowship (FP7-PEOPLE-2012-IEF) project ECOCHEM. G. P. would like to thank the Ministry of Education and Religious Affairs in Greece for the financial support of this work provided under the co-operational program "AdvePol: E850". The authors gratefully acknowledge the support of the Cluster of Excellence "Engineering of Advanced Materials" at the University of Erlangen-Nuremberg, which is funded by the German Research Foundation (DFG) within the framework of its "Excellence Initiative", Synthetic Carbon Allotropes (SFB953) and Solar Technologies go Hybrid (SolTech).

References

1. Brabec, C. J., Sariciftci, N. S., & Hummelen, J. C. Plastic Solar Cells. *Adv. Funct. Mater.* **11** (1), 15-26 (2001).
2. Vohra, V., *et al.* Efficient inverted polymer solar cells employing favourable molecular orientation. *Nat. Photon.* **9**, 403-408 (2015).
3. He, Z., *et al.* Single-junction polymer solar cells with high efficiency and photovoltage. *Nat. Photon.* **9** (3), 174-179 (2015).
4. Chen, J.-D., *et al.* Single-Junction Polymer Solar Cells Exceeding 10% Power Conversion Efficiency. *Adv. Mater.* **27** (6), 1035-1041 (2014).
5. Liu, Y., *et al.* Aggregation and morphology control enables multiple cases of high-efficiency polymer solar cells. *Nat. Commun.* **5** (9), 5293 (2014).
6. Po, R., Carbonera, C., Bernardi, A., & Camaioni, N. The role of buffer layers in polymer solar cells. *Energy Environ. Sci.* **4** (2), 285 (2011).
7. Ameri, T., Dennler, G., Lungenschmied, C., & Brabec, C. J. Organic tandem solar cells: A review. *Energy Environ. Sci.* **2** (4), 347 (2009).
8. Ameri, T., Li, N., & Brabec, C. J. Highly efficient organic tandem solar cells: a follow up review. *Energy Environ. Sci.* **6** (8), 2390-2413 (2013).
9. You, J., *et al.* A polymer tandem solar cell with 10.6% power conversion efficiency. *Nat. Commun.* **4**, 1446 (2013).
10. Guo, F., *et al.* Solution-Processed Parallel Tandem Polymer Solar Cells Using Silver Nanowires as Intermediate Electrode. *ACS Nano* **8** (12), 12632-12640 (2014).
11. Chen, C.-C., *et al.* An Efficient Triple-Junction Polymer Solar Cell Having a Power Conversion Efficiency Exceeding 11%. *Adv. Mater.* **26** (32), 5670-5677 (2014).
12. Ameri, T., Khoram, P., Min, J., & Brabec, C. J. Organic ternary solar cells: A review. *Adv. Mater.* **25**, 4245-4266 (2013).
13. Koppe, M., *et al.* Near IR Sensitization of Organic Bulk Heterojunction Solar Cells: Towards Optimization of the Spectral Response of Organic Solar Cells. *Adv. Funct. Mater.* **20** (2), 338-346 (2010).
14. Ameri, T., *et al.* Performance enhancement of the p3ht/pcbm solar cells through nir sensitization using a small-bandgap polymer. *Adv. Energy Mater.* **2**, 1198-1202 (2012).
15. Guo, F., *et al.* A generic concept to overcome bandgap limitations for designing highly efficient multi-junction photovoltaic cells. *Nat. Commun.* **6**, 7730 (2015).
16. Gasparini, N., *et al.* An Alternative Strategy to Adjust the Recombination Mechanism of Organic Photovoltaics by Implementing Ternary Compounds. *Adv. Energy Mater.* (2015).
17. Spyropoulos, G. D., *et al.* Flexible organic tandem solar modules with 6% efficiency: combining roll-to-roll compatible processing with high geometric fill factors. *Energy Environ. Sci.* **7** (10), 3284-3290 (2014).
18. Li, N., *et al.* Towards 15% energy conversion efficiency: a systematic study of the solution-processed organic tandem solar cells based on commercially available materials. *Energy Environ. Sci.* **6** (12), 3407-3413 (2013).
19. Lu, L., Chen, W., Xu, T., & Yu, L. High-performance ternary blend polymer solar cells involving both energy transfer and hole relay processes. *Nat. Commun.* **6**, 7327 (2015).
20. Yang, Y. M., *et al.* High-performance multiple-donor bulk heterojunction solar cells. *Nat. Photon.* **9** (3), 190-198 (2015).
21. Zhang, Y., *et al.* Synergistic Effect of Polymer and Small Molecules for High-Performance Ternary Organic Solar Cells. *Adv. Mater.* **27** (6), 1071-1076 (2015).
22. Ameri, T., *et al.* Morphology analysis of the near IR sensitized polymer / fullerene organic solar cells by implementing low bandgap polymer analogous of C-/Si-PCPDTBT. *J. Mater. Chem. A* **2**, 19461-19472 (2014).
23. Cheng, P., Li, Y., & Zhan, X. Efficient ternary blend polymer solar cells with indene-C60 bisadduct as an electron-cascade acceptor. *Energy Environ. Sci.* **7** (6), 2005 (2014).
24. Khlyabich, P. P., Rudenko, A. E., Street, R. A., & Thompson, B. C. Influence of Polymer Compatibility on the Open-Circuit Voltage in Ternary Blend Bulk Heterojunction Solar Cells. *ACS Appl. Mater. Interfaces.* **6** (13), 9913-9919 (2014).
25. Lu, L., Xu, T., Chen, W., Landry, E. S., & Yu, L. Ternary blend polymer solar cells with enhanced power conversion efficiency. *Nat. Photon.* **8** (9), 716-722 (2014).
26. Lim, B., Bloking, J. T., Ponec, A., Mcgehee, M. D., & Sellinger, A. Ternary Bulk Heterojunction Solar Cells: Addition of Soluble NIR Dyes for Photocurrent Generation beyond 800 nmDyes for Photocurrent Generation beyond 800 nm. *ACS Appl. Mater. Interfaces.* **6**, 6905 (2014).

27. Itskos, G., *et al.* Optical properties of organic semiconductor blends with near-infrared quantum-dot sensitizers for light harvesting applications. *Adv. Energy Mater.* **1** (5), 802-812 (2011).
28. Mulherin, R. C., *et al.* Ternary photovoltaic blends incorporating an all-conjugated donor-acceptor diblock copolymer. *Nano Lett.* **11** (11), 4846-4851 (2011).
29. Savoie, B. M., Dunaisky, S., Marks, T. J., & Ratner, M. a. The Scope and Limitations of Ternary Blend Organic Photovoltaics. *Adv. Energy Mater.* **5** (3), 1400891 (2015).
30. Gasparini, N., *et al.* Photophysics of Molecular-Weight-Induced Losses in Indacenodithienothiophene-Based Solar Cells. *Adv. Funct. Mater.* **25** (30), 4898-4907 (2015).
31. Heumueller, T., *et al.* Disorder-Induced Open-Circuit Voltage Losses in Organic Solar Cells During Photoinduced Burn-In. *Adv. Energy Mater.* (2015).
32. Pivrikas, A., Sariciftci, N. S., Juška. G., and Österbacka, R. A Review of Charge Transport and Recombination in Polymer / Fullerene. *Progr. Photovoltaics: Res. Appl.* **15**, 677-696 (2007).
33. Clarke, T. M., Lungenschmied, C., Peet, J., Drolet, N., & Mozer, A. J. A Comparison of Five Experimental Techniques to Measure Charge Carrier Lifetime in Polymer/Fullerene Solar Cells. *Adv. Energy Mater.* **5** (4) (2014).
34. Min, J., *et al.* Effects of Alkyl Terminal Chains on Morphology, Charge Generation, Transport, and Recombination Mechanisms in Solution-Processed Small Molecule Bulk Heterojunction Solar Cells. *Adv. Energy Mater.* **5** (17) (2015).
35. Shuttle, C. G., *et al.* Experimental determination of the rate law for charge carrier decay in a polythiophene: Fullerene solar cell. *Appl. Phys. Lett.* **92** (2008), 90-93 (2008).
36. Street, R. a., Krakaris, A., & Cowan, S. R. Recombination through different types of localized states in organic solar cells. *Adv. Funct. Mater.* **22**, 4608-4619 (2012).
37. Azimi, H., Senes, A., Scharber, M. C., Hingerl, K., & Brabec, C. J. Charge Transport and Recombination in Low-Bandgap Bulk Heterojunction Solar Cell using Bis-adduct Fullerene. *Adv. Energy Mater.* **1** (6), 1162-1168 (2011).
38. Salvador, M., *et al.* Electron accumulation on metal nanoparticles in plasmon-enhanced organic solar cells. *ACS Nano* **6** (11), 10024-10032 (2012).
39. Noone, K. M., *et al.* Photoinduced charge transfer and polaron dynamics in polymer and hybrid photovoltaic thin films: Organic vs inorganic acceptors. *J. Phys. Chem. C* **115** (49), 24403-24410 (2011).
40. Gasparini, N., *et al.* Neat C70 -Based Bulk-Heterojunction Polymer Solar Cells with Excellent Acceptor Dispersion. *Appl. Mater. Interfaces* **6**, 21416-21425 (2014).

